doi: 10.1111/j.1600-0854.2009.00950.x

Involvement of Vps33a in the Fusion of Uroplakin-Degrading Multivesicular Bodies with Lysosomes

Xuemei Guo[1], Liyu Tu[1], Iwona Gumper[1], Heide Plesken[1], Edward K. Novak[2], Sreenivasulu Chintala[2], Richard T. Swank[2], Gregory Pastores[3], Paola Torres[3], Tetsuro Izumi[4], Tung-Tien Sun[1,5,6,7,8], David D. Sabatini[1,8] and Gert Kreibich[1,8,*]

[1]Department of Cell Biology, New York University School of Medicine, 550 First Avenue, New York, NY 10016, USA
[2]Department of Molecular and Cellular Biology, Roswell Park Cancer Institute, Buffalo, NY 14263, USA
[3]Department of Neurology, New York University School of Medicine, 550 First Avenue, New York, NY 10016, USA
[4]Department of Molecular Medicine, Gunma University, Maebashi, Japan
[5]Department of Pharmacology, New York University School of Medicine, 550 First Avenue, New York, NY 10016, USA
[6]Department of Urology, New York University School of Medicine, 550 First Avenue, New York, NY 10016, USA
[7]Department of Epithelial Biology Unit, The Ronald O. Perelman Department of Dermatology, New York University School of Medicine, 550 First Avenue, New York, NY 10016, USA
[8]Department of NYU Cancer Institute, New York University School of Medicine, 550 First Avenue, New York, NY 10016, USA
**Corresponding author: Gert Kreibich, gert.kreibich@nyumc.org*

The apical surface of the terminally differentiated mouse bladder urothelium is largely covered by urothelial plaques, consisting of hexagonally packed 16-nm uroplakin particles. These plaques are delivered to the cell surface by fusiform vesicles (FVs) that are the most abundant cytoplasmic organelles. We have analyzed the functional involvement of several proteins in the apical delivery and endocytic degradation of uroplakin proteins. Although FVs have an acidified lumen and Rab27b, which localizes to these organelles, is known to be involved in the targeting of lysosome-related organelles (LROs), FVs are CD63 negative and are therefore not typical LROs. Vps33a is a Sec1-related protein that plays a role in vesicular transport to the lysosomal compartment. A point mutation in mouse Vps33a (Buff mouse) causes albinism and bleeding (Hermansky-Pudlak syndrome) because of abnormalities in the trafficking of melanosomes and platelets. These Buff mice showed a novel phenotype observed in urothelial umbrella cells, where the uroplakin-delivering FVs were almost completely replaced by Rab27b-negative multivesicular bodies (MVBs) involved in uroplakin degradation. MVB accumulation leads to an increase in the amounts of uroplakins, Lysosomal-associated membrane protein (LAMP)-1/2, and the activities of β-hexosaminidase and β-glucocerebrosidase. These results suggest that FVs can be regarded as specialized secretory granules that deliver crystalline arrays of uroplakins to the cell surface, and that the Vps33a mutation interferes with the fusion of MVBs with mature lysosomes thus blocking uroplakin degradation.

Key words: bladder epithelium, fusiform vesicles, Hermansky-Pudlak syndrome, lysosome-related organelles, organelle biogenesis, secretory granules, uroplakins, urothelium, Vps33a

Received 24 November 2008, revised and accepted for publication 21 May 2009, uncorrected manuscript published online 26 May 2009

The urinary bladder and much of the rest of the lower urinary tract are lined by a unique type of stratified epithelium, called urothelium, which is characterized by a surface layer of highly specialized, terminally differentiated umbrella cells (1–3). The apical surface of these cells is almost completely covered by urothelial plaques [also known as asymmetric unit membranes (AUMs)] (1,4), which are 2D crystals of hexagonally packed 16-nm particles (4–8) composed of four major transmembrane proteins, the uroplakins (UPs) Ia, Ib, II and IIIa (9–15). The assembly process of UPs begins in the endoplasmic reticulum (ER) (16,17), where specific UPIa/II and UPIb/III heterodimers are formed (12–14,16,17). Small crystalline arrays of 16-nm UP particles are first observed in the *trans* Golgi network (TGN) (18), from which a population of discoidal vesicles is derived and in which the crystalline UP plaques accumulate and expand (1,2,4,8,9,16). When these plaques cover the entire surface the vesicles acquire a somewhat flattened disc configuration, leading to their designation as fusiform vesicles (FVs) (1,4).

Mature FVs occupy large portions of the apical cytoplasm of the umbrella cells where, in response to signals presumably related to bladder distention, they undergo fusion with the apical plasma membrane to deliver the crystalline plaques (19–23). It has long been thought that FVs could also be formed by retrieval of urothelial plaques from the apical surface of umbrella cells, and that this bidirectional movement provides a means to reversibly modulate the surface area of the urothelium in response to changes in bladder volume (18–21,24). This notion was supported by reports that stretching of the bladder led to a significant decrease in the number of cytoplasmic FVs (19,21) and

to an increase in urothelial apical surface area based on electrophysiological measurements (24). Whether recycling of surface AUMs via FVs actually takes place during the micturition cycle has been questioned, as UPs internalized from the plasma membrane appeared to be subsequently degraded in lysosomal compartments (21,25).

Previously, we showed that Rab27b, a member of the Rab family of small GTP binding proteins known to play a role in organelle targeting (26,27), is highly expressed in the urothelial umbrella cells where it is associated with FVs (22) . Furthermore, Rab27b and/or its close homolog Rab27a have been shown to be involved in the targeting and the regulated plasma membrane fusion not only of secretory granules (28,29) but also of some lysosome-related organelles (LROs; also known as secretory lysosomes) (30–32). The LROs are cell-type specific organelles that have a variety of functions and share some compositional and physiological characteristics with conventional lysosomes (33–36). The family of LROs includes melanosomes, dense core granules of platelets, lytic granules of cytotoxic T lymphocytes (CTLs), mast cell basophilic granules, Weibel-Palade bodies of endothelial cells and azurophilic granules of neutrophils or eosinophils (33,35,36). It is interesting to note that also Rab11a plays a role in the exocytosis of FVs (37).

Vps33a is a Sec1-related protein involved in vesicular transport to the lysosomal compartment, and it is a protein of the homotypical vacuolar protein sorting (HOPS) complex that is involved in the regulation of endosome-lysosome fusion (38,39). A point mutation in mouse Vps33a (Asp251Glu) causes albinism and prolonged bleeding because of abnormalities in melanocyte, platelet trafficking (39). This mouse (known as the Buff mouse) provides a model system for Hermansky-Pudlak syndrome (HPS) (40), which is an autosomal recessive disorder caused by mutations in proteins, including Vps33a, that regulate the trafficking of LROs (31,35,41–44). The Buff mouse and several other mouse models for this syndrome have been characterized and have helped to identify the specific function of some of the cognate regulatory proteins (31,43,44).

Here we demonstrate that the Rab27b-associated FVs have an acidified lumen, and those immature FVs, but not the mature ones, contain CD63. In addition, we show that the Vps33a mutation has a novel phenotype in urothelial umbrella cells by causing a marked depletion of FVs and a concomitant accumulation of large amounts of multivesicular body (MVB)-like organelles. The large amounts of MVB-like organelles accumulating in umbrella cells of the Vps33a mutant mouse were noted to be a part of the degradative pathway. As protein sorting into MVBs and delivery to the lysosomal lumen are the major mechanisms for degrading post-Golgi integral membrane proteins in all eukaryotic cells (45), our results indicate that the mutation of Vps33a leads to the diversion of a large fraction of urothelial plaques into a degradative pathway where they accumulate in MVBs. The resulting expansion of this late endosomal compartment is most likely because of its inability to fuse with mature lysosomes.

Results

The fusiform vesicles are acidified and do not contain CD63

We have previously shown that high levels of Rab27b are expressed in urothelial umbrella cells where they are bound to FVs (22). In many non-urothelial tissues, the expression of Rab27b is associated with the biogenesis and/or trafficking of secretory granules (28,29) and LROs (30,32,36). We therefore decided to characterize the Rab27b-positive FVs more closely and to determine whether FVs are LROs. Incubation of mouse bladder explants with acridine orange led to the staining of numerous cytoplasmic vesicles that were largely restricted to the cytoplasm of umbrella cells (Figure 1A). Similar results were obtained using another weak base, 4-dinitroanilino-3′-amino-*N*-methyldipropylamine (DAMP) (46), showing intense green labeling with a granular appearance in the apical cell layer corresponding to the umbrella cells (Figure 1C). On the other hand, immunolabeling using anti-LAMP-1 antibodies showed that lysosomes or late endosomes are rather evenly distributed in all cell layers of the urothelium (Figure 1B). Therefore, most of the acidified organelles labeled by acridine orange and DAMP in umbrella cells do not correspond to lysosomal or late endosomal compartments, but correspond to the very abundant population of FVs. At the electron microscopic (EM) level (Figure 1D,E), the gold particles representing DAMP are not only found over the lumen of lysosomes (Lys) but also over FVs, which become dilated under mild fixation conditions. Together, these findings indicate that FVs have an acidified lumen, a property not only shared by lysosomal compartments but also by secretory granules and LROs (33,47).

The tetraspanin CD63 had been demonstrated to be a reliable marker for LROs (47). Immunolabeling of mouse bladder sections with an anti-CD63 antibody showed that umbrella cells, which contain essentially all the mature FVs, show no significant labeling, indicating that mature FVs do not contain CD63 (Figure 2). Some punctate labeling was observed in the urothelial cell layer below the umbrella cells, and some of these structures were also UPIII-positive (arrows in Figure 2), indicating that immature FVs may be at least transiently CD63-positive. These results also indicate that mature FVs most likely do not correspond to LROs, but represent instead a special type of secretory granules that deliver membranes containing UPs in a highly concentrated, crystalline form to the apical surface of the umbrella cells.

Umbrella cells of the Buff mouse lack FVs but accumulate MVB-like vacuoles

Because the biogenesis and targeting of LROs such as melanosomes and platelet dense granules are altered in

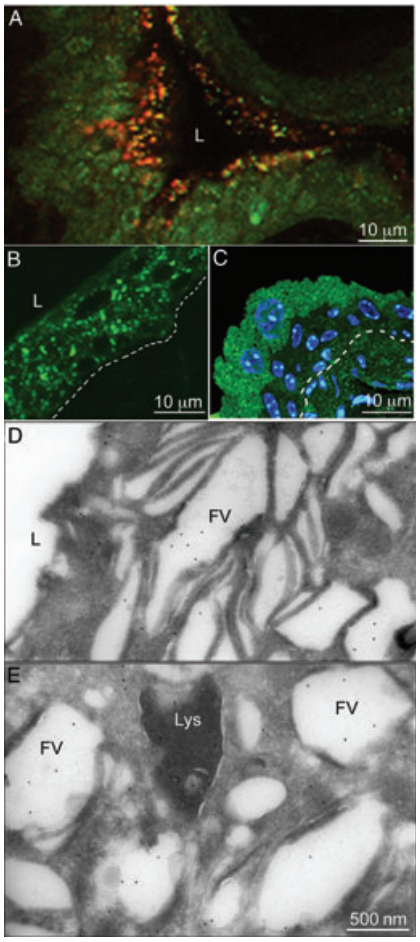

Figure 1: The lumen of umbrella cell FVs are acidified. A) Acridine orange staining of mouse urothelium. Mouse bladder explants were incubated with acridine orange and the fluorescent reagent accumulating in acidified compartments was detected by its characteristic orange emission by fluorescence microscopy. B) Immunostaining of mouse bladder sections with an anti-LAMP-1 antibody. C) Immunolocalization of DAMP on frozen sections from a mouse bladder incubated *in situ* with DAMP by immunofluorescence. At the ultrastructural level (D and E), gold-conjugated protein A was used. L indicates the lumen of the bladder. The location of the urothelial basement membrane is indicated by a dashed line in (B) and (C). Note acridine orange (A) and DAMP (green, C) accumulated predominantly in umbrella cells, while LAMP-1 staining (B) was rather evenly distributed in all layers of the urothelium. In panels (D and E), DAMP localized mainly to FVs (FV) and to lysosomes (Lys).

the Buff mouse (39), we wondered whether urothelial FVs were also affected. Unlike the cytoplasm of wild-type umbrella cells, which is mainly occupied by mature FVs interspersed by small vesicles, mitochondria and a few large vacuoles (Figures 3A,B and S1), umbrella cells of the Buff mouse urothelium contained few FVs and were filled with large MVB-like vacuoles, creating a foam-like appearance (Figures 3C,D and S2). This phenotype was observed in essentially all umbrella cells of the Buff mouse. Despite the depletion of FVs, the apical plasma membrane of Buff mouse umbrella cells (Figure 3F) had the typical AUM appearance seen in control mice (Figure 3E), indicating that the available FVs were sufficient to deliver crystalline plaques of UPs to cover the apical membrane. Examination of the umbrella cells of an 8-day-old Buff mouse (Figure 3G) showed a less severe phenotype when compared with that of 3-month-old adult mice (Figure 3D), i.e. there are still some FVs found concentrated beneath the apical plasma membrane, and the accumulation of the MVB-like vacuoles was less pronounced. These observations indicate that the phenotype seen in Buff mice is age-dependent.

The MVB-like vacuoles are involved in the endocytic degradative pathway of uroplakins

To investigate whether the MVB-like vacuoles were FV related, we examined the ultrastructure of Buff mouse umbrella cells (Figure 4). The membranes forming these MVB-like vacuoles have an angular appearance (Figure 4A), similar to that of the apical plasma membranes of umbrella cells and FVs. The MVB-like vacuoles contained amorphous material (Figure 4A) or various numbers of small vesicles with an average diameter of 40 nm (Figure 4C,D,E). Variations in morphology of the vacuole contents most likely reflect different stages in MVB maturation (48). That typical AUM structures (Figure 4B) can be clearly identified in these MVB-like vacuoles suggests that they are FVs related and that they are most likely part of the degradative pathway for UP plaque components.

Fibroblasts in the extracellular matrix space below the urothelium also showed morphological abnormalities. In normal fibroblasts, the rough ER is the predominant organelle (Figures S1 and S3A), whereas in the Buff mouse fibroblasts are filled with vacuolar structures containing undigested material (Figures S2 and S3B), a phenotype seen in lysosomal storage diseases (49). Similar morphological changes were observed in the pancreatic fibroblasts of Buff mice (not shown). Because the functions of regular late endosomes/lysosomes are affected in this mouse model of HPS, the observed phenotype in umbrella cells does not support the argument that FVs are LROs. It appears that in umbrella cells inhibition of the pathway toward degradation in mature lysosomes caused by the mutation in Vps33a resulted in the accumulation of urothelial plaques in MVBs, while in fibroblasts, presumably undigested extracellular matrix components forming multilamellar structures filled the cytoplasm. Although Vps33a is thought to be ubiquitously expressed (50), and the Vps33a mutation led to severe phenotypes in umbrella cells and bladder fibroblasts, this mutation did not affect the appearance of typical secretory granules of the exocrine and endocrine pancreas (not shown), suggesting that the former bladder cell types have a much more active endocytic/degradative pathway.

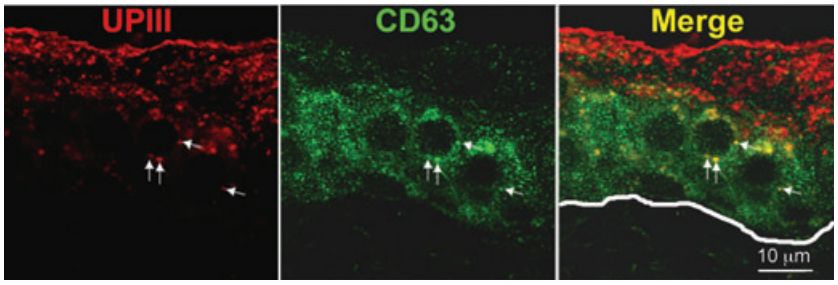

Figure 2: Mature FVs do not contain CD63. Paraffin sections of bladders from wild-type mice were immunostained with antibodies against UPIII (red) and CD63 (green). There is very little CD63 expressed in umbrella cells where most of the mature FVs are located. Arrows indicate colocalization of UPIII and CD63 in the intermediate cell layers. The line in the Merge panel indicates the location of the basal lamina.

As shown earlier for wild-type mice, UPIII and Rab27b are most strongly expressed in urothelial umbrella cells, with the highest concentrations found just underneath the apical plasma membrane (Figure 5A,B) (22). The expression of these two differentiation markers are grossly altered in the Buff mouse urothelium: UPIII concentrations are greatly increased in most umbrella cells (D), corresponding to increased levels of MVB-like vacuoles, while the expression of Rab27b is significantly lower (E), which is apparently related to the disappearance of FVs (Figures 3D and S2). Immunogold labeling on frozen sections showed that in control mice, UPIII localized predominantly to FVs in umbrella cells (Figure 6A). It also demonstrated that the MVB-like vacuoles in Buff mouse umbrella cells contained UPIII (Figure 6B), which was found to be associated not only with the limiting membranes of the MVB-like vacuoles but also with the amorphous material and small vesicles contained in the

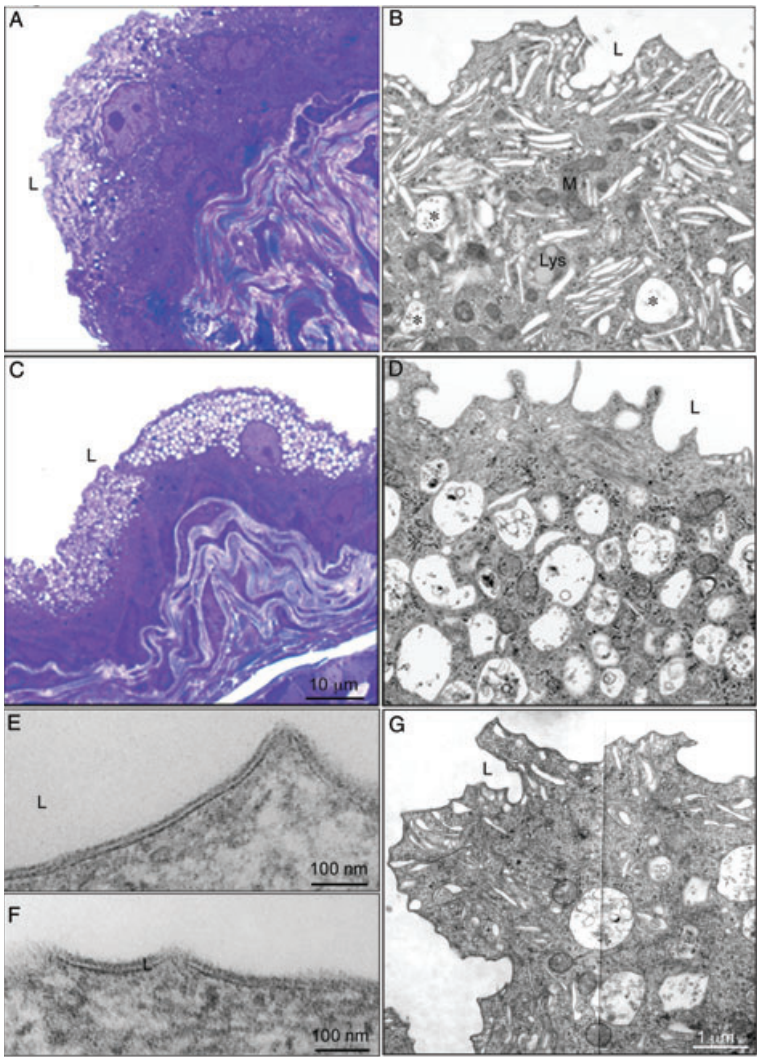

Figure 3: Mutation of Vps33a in the Buff mouse results in the accumulation of numerous MVB-like vacuoles in urothelial umbrella cells. Light micrographs of normal (A) and Buff mouse (C) urinary bladders, embedded in epon and stained with toluidine blue. While normal urothelial umbrella cells (A) have few vacuoles, those from the Buff mouse (C) are highly vacuolated. Panels (B) and (D) represent magnified areas from the overview EMs shown in Figures S1 and S2 of the Supporting Information. Asterisks in panel B indicate MVBs in umbrella cells of normal urothelium. Panels (E) and (F) are higher magnification images of the apical plasma membrane of control and Buff mouse umbrella cells, respectively, showing the typical AUM appearance. G) Apical portion of an umbrella cell from an 8-day-old Buff mouse where FVs are still the predominant organelles.

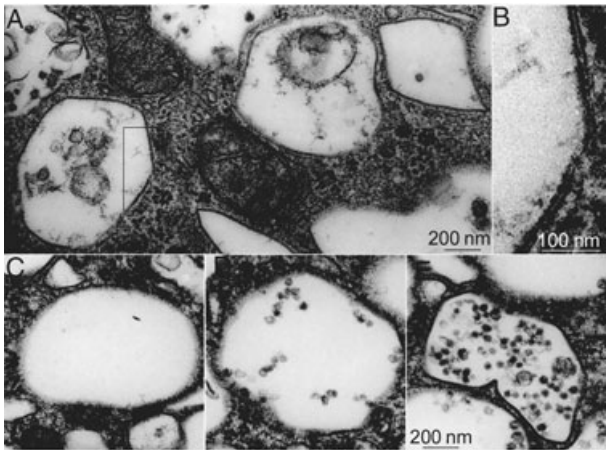

Figure 4: The MVB-like vacuoles in umbrella cells of Buff mice are related to FVs and belong to the degradative pathway. Gallery of electron micrographs of cytoplasmic vacuoles in Buff mouse umbrella cells. A) The MVB-like vacuoles have rather angular contours, indicating a certain rigidity of the limiting membranes. B) At higher magnification, the asymmetric unit membrane (AUM) structure, typical of FVs and of the apical plasma membrane of normal umbrella cells, can also be seen in these MVB-like vacuoles. C–E) The luminal contents of these large MVB-like vacuoles differ widely.

lumen of these vacuoles (arrows). Consistent with the immunofluorescence results, we found that in contrast to normal umbrella cells, where Rab27b is localized predominantly to FVs, the MVB-like vacuoles in Buff mouse cells were labeled only by few gold particles (arrows in Figure 6D). The increased expression levels of UPIII and Rab27b in the intermediate cell layer of the Buff mouse suggest that these cells differentiate prematurely and target FVs to their plasma membranes by a mechanism that presumably involves Rab27b. This conclusion is also supported by immunogold double labeling experiments showing that vesicles in the cell layer below the umbrella cells contain both Rab27b and UPIII (Figure S4).

To further characterize the large vacuoles accumulating in Buff mouse umbrella cells, we immunostained bladder sections of wild-type and Buff mice using antibodies directed against the late endosomal/lysosomal markers, LAMP-1 (Figure 5H,K, respectively) and LAMP-2 (not shown). In the wild-type mouse, both LAMP-1 (Figure 5H) and LAMP-2 (not shown) were found in all urothelial layers, with somewhat higher levels of expression in the lower cells. While in normal urothelium these lysosomal markers did not colocalize with UPIII (for LAMP-1, see Figure 5G–I; see also Figure 6A,F), in the Buff mouse they had a similar cellular distribution as UPIII (Figure 5J–L; see also Figure 6B,F). The merged images also suggest significant heterogeneity in protein expression, which may represent different levels of accumulations of MVB-like organelles (see also Figures S2 and 5K). EM analysis of normal umbrella cells showed that LAMP-1 were associated with lysosomes (Figure 6E), but in the Buff mouse they were associated, in addition with the limiting membrane as well as some luminal materials of the MVB-like vacuoles (Figure 6F). The colocalization of UPIII and LAMP1/2 in MVBs supports the idea that these organelles are involved in the degradation of AUMs that may be derived from the apical plasma membrane or from FVs (see also Figure 8).

Vps33a mutation prevents fusion of MVBs with lysosomes

A likely explanation for the accumulation of MVB-like organelles in the Buff mouse is that the fusion of MVBs with lysosomes is blocked because of the Vps33a mutation. Consistent with such a mechanism are western blot results (Figure 7), which showed a large increase in the content of UPII (450%) and UPIII (320%). There were similar accumulations of the two lysosomal markers LAMP-1 and -2, and a modest increase in Rab27b (150%). Loading onto the gels constant amounts of protein, the specific content of actin in the urothelium of Buff mice was consistently lower (50–60%). Therefore, normalization based on constant actin content would increase the accumulation of UPs even further. Because urothelial

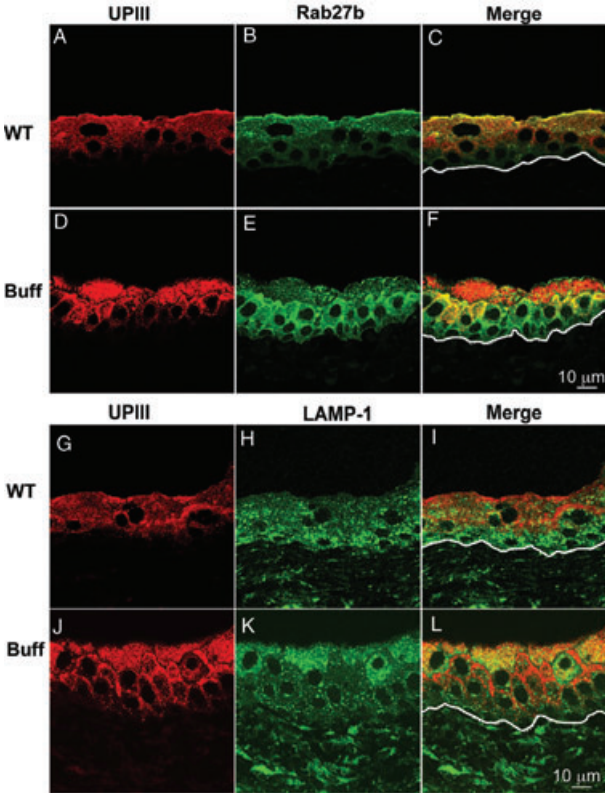

Figure 5: Changed expression pattern of UPIII, Rab27b and LAMP-1 in umbrella cells of Buff mice. Paraffin sections of bladders from wild-type (WT; A–C, G–I) or Buff mice (Buff; D–F, J–L) were immunostained with antibodies against UPIII (A,D,G,J), Rab27b (B,E) or LAMP-1 (H,K). The line in the 'Merge' panels indicates the location of the basal lamina.

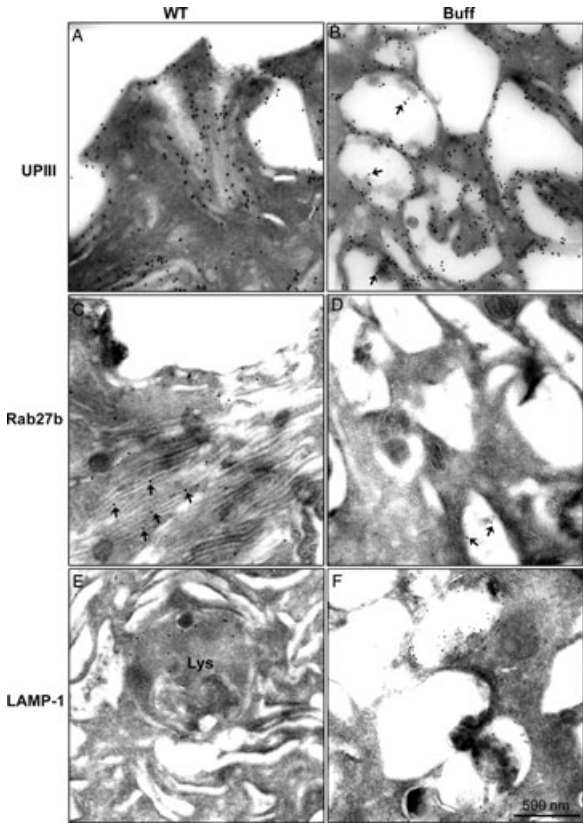

Figure 6: The large MVB-like vacuoles in umbrella cells of Buff mice are UPIII-positive, Rab27b-negative and LAMP-1-positive. Frozen thin sections of the bladder of WT (WT; A,C,E) and Buff mice (Buff; B,D,F) were immunogold labeled using primary antibodies against UPIII (A,B), Rab27b (C,D) or LAMP-1 (E,F). Note that the large MVB-like vacuoles in umbrella cells of Buff mice contain LAMP-1 and UPIII, but not Rab27b. Asterisks in panel B indicate UPIII associated with intraluminal vesicles of MVBs. Asterisks in panel C indicate Rab27b localized to fusiform vesicles. Asterisks in panel D indicate that Rab27b is rarely detected in MVBs.

umbrella cells of the Buff mouse lacked FVs (Figures 3D and S2) that were replaced by MVBs, the observed increase in UPII and UPIII levels is most likely because of the accumulation of UPs in the MVBs.

It is interesting to note that the urothelial phenotype of the lysosomal integral membrane protein (LIMP)-2 knockout (KO) mouse is similar to that of the Buff mouse (51). LIMP-2 is an integral membrane protein found normally in late endosomes/MVBs and in mature lysosomes (52). Recently, this protein has been identified as the receptor that functions in the vesicular transport of β-glucocerebrosidase (β-GC) from the TGN to late endosomes (53). This raised the possibility that Vps33a and the associated HOPS complex may play a role in the delivery of lysosomal enzymes to late endosomes, and that a defect in Vps33a may lead to lower levels of enzymes needed for UP degradation. In such a scenario, one would also expect a phenotype akin to a lysosomal storage disorder, which is characterized by the accumulation of undigestible material in lysosomes or MVBs. Although UPs are not substrates for β-GC, it is possible that other lysosomal enzymes, that affect the degradation of UPs, use the same receptor for their delivery to late endosomal compartments. We, therefore, measured the β-GC and β-hexosaminidase (β-Hex; transported by the mannose-6-phosphate receptor) levels in urothelial and liver homogenates of control and Buff mice (Table 1). In contrast to the LIMP-2 KO mouse, where β-GC levels in the liver were less than 10% of those in wild-type mice (53), in Buff mice the β-GC levels in the liver were not significantly different. In the urothelium of Buff mice this enzyme activity was even somewhat elevated compared with wild-type mice, although this difference is not significant. These findings reinforce our conclusion that Vps33a functions in a step affecting the maturation of MVBs such as the fusion of MVBs with mature lysosomes (48). The persistent presence of a small number of MVB-like structure in wild-type umbrella cells (Figures 3B and S1) (1) indicates that MVBs are intermediates in the degradative pathway for AUMs that function also in the normal urothelium.

Discussion

In urothelial umbrella cells, FVs function as storage organelles for AUMs that may be inserted in a regulated manner into the apical membrane (2,19–23). Our findings suggest that FVs are also linked to the endocytic/lysosomal pathway, but are most likely not related to LROs. We have previously shown that FVs are associated with Rab27b (22), a small GTPase that is not only associated with secretory granules (28,29) but also with LROs (29,30,32). The finding that FVs have an

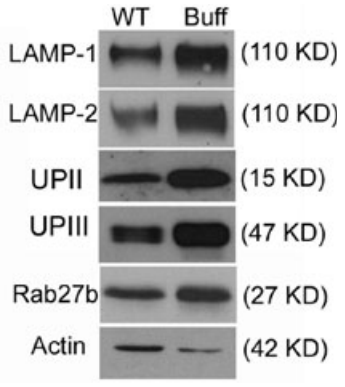

Figure 7: The urothelium of Buff mice contains higher concentrations of LAMP-1, LAMP-2, uroplakins and Rab27b. Fifty micrograms each of total urothelial proteins obtained from wild-type (WT) or Buff (Buff) mice were separated by SDS–PAGE, and immunoblotted using antibodies against LAMP-1, LAMP-2, UPII, UPIII, Rab27b or actin. Note the significant increase in the relative amounts of both uroplakins and the LAMPs in the urothelium of the Buff mouse when compared with that of WT bladder urothelium.

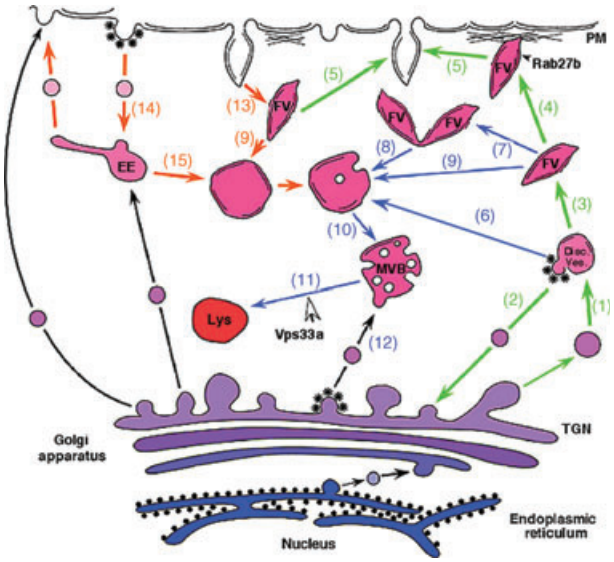

Figure 8: Schematic representation of an urothelial umbrella cell. Emphasized are likely steps (1–15) involved in the biogenesis and targeting of FVs as well as in their degradation. The green arrows indicate steps involved in the biogenesis and exocytosis of FVs, whereas the orange ones mark the endocytic pathway affecting AUMs (see also the introductory paragraph). Blue arrows connect steps that function in the formation of lysosomes. Our results suggest that Vps33a functions in step (11) that is involved in the fusion of MVBs with mature lysosomes (Lys), but not in step (12) that regulates the delivery of lysosomal enzymes to late endosomes or MVBs. Inhibition of step (11) caused by the point mutation in Vps33a is most likely responsible for the accumulation of UPs that are contained in the MVBs.

Table 1: Activities of lysosomal enzymes are elevated in the Buff mouse urothelium

Mouse strain	Liver		Urothelium	
	β-Hex[a]	β-GC[a]	β-Hex[a]	β-GC[a]
Wild-type	118 ± 64	162 ± 81	887 ± 368	267 ± 133
Buff	136 ± 93	119 ± 9	1947 ± 313	375 ± 107

[a] β-Hexosaminidase (β-Hex) and β-glucocerebrosidase (β-GC) activities are expressed as nanomoles of substrate hydrolyzed/mg protein/h at 37°C. ($\alpha = 0.05, n = 3$). The two-group t-test was used to compare enzyme activities. The β-Hex activity in urothelium of Buff mice was significantly higher ($p > 0.05$) than that in wild-type mice, while no significant difference ($p < 0.05$) in the β-GC activity was observed when wild-type and Buff mice are compared. Also enzyme activities in the liver were not significantly different in wild-type and mutant mice.

acidified lumen (Figure 1) is compatible with their being a secretory granule-like organelle or a LRO. However, we found that CD63, a marker for LROs (47), is not associated with FVs. Our results thus suggest that FVs are not typical LROs, but rather represent a highly specialized secretory granule-type organelle that inserts membrane proteins (UPs) in a highly concentrated, crystalline form into the apical surface of umbrella cells. In the Buff mouse, where LROs in several cell types are affected by a point mutation in Vps33a (39), FVs disappear almost completely from umbrella cells and are replaced by degradative organelles, most notably by the MVB-like vacuoles. Although Vps33a is ubiquitous (50), the fact that cells of the endocrine and exocrine pancreas are not affected in the Buff mouse (not shown) indicates that FVs are in this regard distinct from these *bona fide* secretory granules. This difference may reflect a much higher endocytic activity of urothelial umbrella cells compared with the pancreatic cells.

Our studies also indicate that MVB-like vacuoles, that are the morphological hallmark of the umbrella cells in the Buff mouse (Figures 3D and S2), are most likely the same ones that are seen at very low levels in normal umbrella cells (Figures 3B and S1). These MVB-like vacuoles are, therefore, related to the normal degradation of UP plaques of the apical plasma membrane that are internalized during the micturition cycles. Alternatively, they are derived from the FVs that are shunted directly into the degradative pathway. As would be expected for MVBs/late endosomes, we found that they are LAMP-1/2-positive (Figures 5 and 6). Supporting their FV origin, these MVB-like vacuoles contain not only UPs but also morphologically recognizable AUMs (Figure 4B). The fact that these MVBs are only seen in the umbrella cell layer, and not in the intermediate or basal cell layer, indicates that their expression is differentiation dependent and related to the apical surface expression of UPs.

The fact that the FVs in the Buff mouse urothelium are almost completely replaced by MVBs can be explained in several ways. First, the Vps33a mutation caused a higher rate of FV fusion with, and retrieval from, the apical umbrella cell membrane. Second, a mechanism that shunts FVs into the endocytic/lysosomal pathway is exaggerated in these cells. The finding that the apical plasma membrane and FVs contain the same SNARE molecules, which would enable FVs to fuse in a homotypic fashion (54), supports this mechanism. Fusion of FVs with organelles of the endocytic pathway would be akin to crinophagy in cells containing secretory granules where, under certain physiological conditions, secretory granules fuse directly with lysosome-related compartments (steps 8 and 9 in Figure 8) (55,56). Third, the Vps33a mutation may activate a feedback mechanism that inhibits synthesis and maturation of new FVs in umbrella cell (57). Fourth, a terminally differentiated umbrella cell may start with a finite complement of FVs that are consumed over the lifetime of the cell. This mechanism is supported by our observation that umbrella cells, even in wild-type mice, may have a heterogenous ultrastructural appearance that may correspond to different stages of their expected life span. Furthermore, in umbrella cells of 8-day-old Buff mice FVs are the most abundant organelles (Figure 3G), suggesting that young umbrella cells still contain a larger pool of FVs that have not been used up. Finally, we cannot rule out the formal possibility that MVBs function in the exocytic pathway and provide in Buff mice a mechanism

for delivering AUMs to the apical surface. Fusion of MVBs with the plasma membrane had been demonstrated in the human erythroleukemia cell line K562. It was shown that fusion of MVBs with the plasma membrane is regulated by Rab11a (58). Interestingly, Rab11a is expressed in urothelial umbrella cells in rather high concentrations and had been shown to function in the fusion of FVs with the apical membrane (37).

A likely interpretation of the accumulation of MVBs in Buff mice is that the mutation in Vps33a interferes with the fusion of MVBs with lysosomes. Vps33a belongs to the Sec1/munc18 family of proteins (39,59), and it is part of the class C Vps complex that includes Vps11, 16, 18, 33a and 41 (60). The components of this complex are highly conserved in yeast and higher eukaryotes, and this complex may function in multiple steps in endocytosis (61), including the SNARE-mediated vesicle docking and fusion with the vacuolar compartment (38,62). In higher eukaryotes, the class C Vps complex plays a role in the biogenesis and intracellular trafficking of melasosomes, and mutations not only in Vps33a but also in Vps16, Vps18 and Vps11 affect the size and number of this organelle (63–66). It appears, therefore, that the mutation in Vps33a prevents the fusion of MVBs with mature lysosomes, resulting in the accumulation of MVBs in umbrella cells. This interpretation would also explain that the Buff mouse urothelium has an increased content of UPs, presumably because of the fact that lysosomal maturation has been blocked, thereby preventing efficient UP degradation. This conclusion is strongly supported by the recent demonstration in Drosophila, that deletion of the Vps33a-encoding *Car* gene results in the accumulation of autopagosome-like structures in the imaginal discs, indicating that fusion of these late endosomal structures with lysosomes requires *Car* (67).

We excluded the possibility that Vps33a, as part of the HOPS complex, plays a role in the delivery of lysosomal enzymes to late endosomes via LIMP-2, the transporter for glucocerebrosidase (53), by demonstrating that the β-glucocerebrosidase activities of wild-type and the Buff mouse urothelium are not significantly different (Table 1). We cannot exclude the possibility, however, that LIMP-2 has in addition a function in the fusion of late endosomes with mature lysosomes as LIMP-2, in contrast to the mannose-6-phosphate receptor, is not only found in the TGN and in endosomal compartments but is also a marker for mature lysosomes (68–70).

The altered morphology of urothelial umbrella cells in the Buff mouse is most likely because of the Vps33a mutation. The possibility that a mutation in another gene did actually cause the MVB accumulation in urothelial umbrella cells is highly unlikely because of the nature of the original buff mutation and because of the system of mating and selection of buff progeny in subsequent generations. The buff mutation occurred as a spontaneous (i.e. single event) mutation on mouse chromosome 5 in the C57BL/6J inbred strain and has subsequently been maintained by repetitive backcrossing to the C57BL/6J wild-type parent. A hypothetical additional mutation elsewhere in the genome of the Buff mouse would have been eliminated by the random chromosome sorting and recombination events occurring during such backcrossing to the wild-type parent. Furthermore, detailed molecular analysis of the region of chromosome 5 including and immediately surrounding the *Vps33a* gene in buff mutants revealed only the Vps33a mutation (39). Although we succeeded in raising rabbit antibodies against recombinant Vps33a, the level of this protein *in vivo* in normal and Buff mouse urothelia was too low to be detected. Therefore, we could not assess whether the level of the mutated form of Vps33a had changed in the Buff mouse urothelium.

Our studies on the urothelium of normal and Buff mice suggest a model for the biosynthesis and targeting of UPs in normal urothelium (Figure 8). This model can explain the disappearance of FVs and the accumulation of MVB-like vacuoles in umbrella cells of the Buff mouse. Early ultrastructural studies suggest that fragments of the TGN containing small AUM assemblies may form discoidal vesicles (DVs) through homotypic fusion (1) (Figure 8, step 1). By cycling membranes back to the TGN that are devoid of AUMs (step 2), the membranes of the DVs would be eventually completely converted into AUMs and assume the flattened morphology typical of mature FVs (step 3). In analogy to melanosomes, FVs may be tethered to cortical actin network (step 4) by a mechanism involving Rab27b together with melanophilin and myosin V (22,71–73). After fusion of FVs with the apical plasma membrane via a specific SNARE complex, AUMs are internalized from the plasma membranes as a result of stretching and relaxing of the bladder during the micturition cycles, either by a retrieval process where FVs are recreated, a mechanism favored by earlier studies (step 13) (2,19,24,74), or by regular endocytosis (step 14) (21). In either case, AUMs accumulate eventually in MVB-like vacuoles (step 10), which then fuse with lysosomes (step 11). In analogy to crinophagy in cells containing secretory granules (56), FVs may even under normal physiological condition fuse at a low rate with elements of the lysosomal apparatus and be converted to MVBs (steps 7–9). The likely reason for the accumulation of MVB-like organelles in umbrella cells of the Buff mouse is that their fusion with mature lysosomes is blocked because Vps33a functions normally in this step (step 11). Such a function of Vps33a is also supported by studies on the corresponding yeast protein where mutations in the *vps*33 gene resulted in morphological changes that affected the functioning of the yeast vacuole, the organelle equivalent to lysosomes in higher eukaryotes (59,60). In fact, Vps33a is a homolog of Sec1p-like regulators of membrane fusion, which in yeast is required for the SNARE-mediated vesicle docking and fusion with the vacuole (61). Although we cannot formally exclude the possibility that MVBs have the capacity to fuse with the apical plasma membrane, the depletion of Rab27b

from umbrella cells of the Buff mouse argues against such a mechanism. Our results indicate that FVs belong to a specialized class of secretory granules, and that the mutation in Vps33a results in the accumulation of MVBs because fusion of this degradative organelle with mature lysosomes is blocked. Our model incorporates our current knowledge on vesicular traffic in urothelial umbrella cells and provides a framework for further studies on membrane trafficking in urothelial umbrella cells.

Materials and Methods

Mice

Wild-type C57BL/6J mice and mutant Buff (*bf/bf*) mice of the same C57BL/6J background were used for all experiments. If not mentioned, otherwise, they were 12–16 weeks of age. The Buff mice were originally from The Jackson Laboratory, subsequently bred at Roswell Park Cancer Institute and then rederived at New York University School of Medicine, Division of Laboratory Animal Resources. All animal protocols were reviewed and approved by the Institutional Animal Care and Use Committees of New York University School of Medicine.

Reagents and antibodies

Acridine orange, DAMP, rabbit anti-dinitrophenyl-KHL IgG, Alexa Fluro® 488 goat anti-rabbit IgG (H+L), Alexa Fluro® 594 goat anti-mouse IgG (H+L), Alexa Fluro® 488 goat anti-rat IgG (H+L) and ProLong® Gold antifade reagent with 4′,6-diamidino-2-phenylindole (DAPI) were from Molecular Probes, Inc. Monoclonal rat anti-mouse LAMP-1 antibody (1D4B) and rat anti-mouse LAMP-2 antibody (ABL-93) were obtained from the Developmental Studies Hybridoma Bank (The University of Iowa, Iowa city, IA). The polyclonal anti-cation-independent mannose-6-receptor (CI-MPR) antibodies are from Affinity Bioreagent. The polyclonal CD63 antibody (H-193) was obtained from Santa Cruz Biotechnology, Inc. The preparation of monoclonal anti-UPIII antibody (75) and polyclonal rabbit anti-Rab27b antibodies (22,76) was previously described. Gold-conjugated goat anti-rat IgG was from Sigma. Normal goat serum was from Zymed Laboratories Inc. Horseradish peroxidase (HRP)-conjugated goat anti-mouse IgG, goat anti-rabbit IgG or goat anti-rat IgG were from Jackson Immuno Research Laboratories, Inc.

Acridine orange staining of mouse urothelium

A fresh mouse bladder was cut into four pieces and incubated with acridine orange solution (5 μg/mL) for 30 min at 37°C in the dark in a buffer containing 140 mM aspartic acid (pH 7.4), 20 mM Hepes (pH 7.4), 5 mM $MgCl_2$, 5 mM EGTA and 5 mM NaCl. After three washes with the same buffer, the bladder pieces were mounted on a slide such that the bladder lumen and the urothelium faced upwards. A rubber ring (diameter 8 mm and 1 mm thick) surrounding the bladder pieces was attached to the slide with grease and covered by a coverslip so that the tissue was covered at all times by the buffer. The sample was immediately viewed on a confocal microscope (LSM 510, Zeiss) with the green and orange filter settings (excitation at 488 nm and emission at 515–530 and 580–630 nm).

DAMP staining of mouse urothelium

DAMP staining was done essentially as described previously (46). A mouse (~30 g) was anesthetized by i.p. injection of a mixture of Xylazine (10 mg/kg body weight) and Ketamine (200 mg/kg body weight), and the mouse abdomen was opened to expose the bladder. About 100 μL of 200 μM DAMP prepared in a special buffer [140 mM aspartic acid (pH 7.4), 20 mM Hepes (pH 7.4), 5 mM $MgCl_2$, 5 mM EGTA and 5 mM NaCl] was directly injected into the bladder. The same amount of this buffer was injected into the bladder of a control mouse. The mouse was placed on a warm plate to maintain its body temperature. After 30 min the mouse was sacrificed and the bladder was excised, rinsed with the buffer, and fixed with 2% paraformaldehyde (PFA) and 0.2% glutaldehyde for 2 h at room temperature. Semi-thin frozen sections (300 nm thick) were cut for immunofluorescence staining of DAMP. Briefly, the sections were incubated first with polyclonal rabbit anti-KHL-DAMP antibody and then with the Alex Fluro® 488 goat anti-rabbit IgG antibody. For immuno-EM localization of DAMP in umbrella cells, ultrathin frozen sections (see below) were incubated with polyclonal rabbit anti-KHL-DAMP antibody and then with gold-conjugated protein A. The samples were viewed and imaged by transmission EM (JEM 200 CX; JEOL).

Immunofluorescence staining

Mouse bladders, fixed in 10% formalin and embedded in paraffin, were sectioned (5 μm thick). After deparaffinization, rehydration and citrate buffer epitope retrieval, sections were blocked with 10% normal goat serum in PGBA buffer (0.1 M PBS, 0.1% gelatin, 1% BSA) and then incubated with primary antibodies such as UPIII (1:1000), Rab27b (1:1000), LAMP-1 (1:20), LAMP-2 (1:20) and CD63 (1:50) at 4°C over night. Alexa Fluro® 488 conjugated goat anti-Rabbit, Alexa Fluro® 594 conjugated goat anti-mouse or Alexa Fluro® 488 conjugated goat anti-rat IgG were used as secondary antibodies. Slides were mounted using the ProLong® Gold antifade reagent and sealed with nail polish. The slides were viewed with the LSM510 confocal microscope (Zeiss).

Enzyme activity assays

From three 8-week-old wild-type and three Buff mice, livers and urothelium were harvested and separately homogenized. β-Glucocerebrosidase and β-hexosaminidase activities were measured using the respective 4-methylumbelliferyl substrates (77).

Electron microscopy

Freshly excised mouse bladders were cut into small pieces (<1 mm^3) and fixed with 2% glutaraldehyde in a 0.1 M cacodylate buffer (pH 7.4) for 2 h at room temperature . The samples were osmicated with 2% osmium tetroxide (OsO_4) in 0.1 M cacodylate buffer (pH 7.4). After staining with 1% uranyl acetate, the samples were embedded in Epon. Semi-thin sections were cut and stained with toluidine blue (1% toluidine blue in 1% sodium borate) and pictured using a light microscope (Axiophot; Carl Zeiss MicroImaging, Inc.). Ultrathin sections were cut for EM.

Immunoelectron microscopy

Small pieces from freshly excised mouse bladders were fixed with 2% PFA /0.2% glutaraldehyde in 0.1 M PHEM buffer (60 mM Pipes, 25 mM Hepes, 10 mM EGTA, 2 mM $MgCl_2$, pH 7.0) for 2 h at room temperature. After washing 3× with PBS and subsequent quenching with 0.02 M glycine in PBS, the samples were infiltrated with 10% gelatin in PBS at 37°C and then solidified on ice. Small blocks were cut from gelatin slabs and transferred to 2.3 M sucrose in PBS over night at 4°C. The blocks were mounted on metal chucks, frozen onto the microtome stub in liquid nitrogen and sectioned on an ultracryomicrotome (Leica Ultra-cut) with cryoattachment. Ultrathin (70–80 nm) frozen sections on a grid were blocked with glycine in PBS for 10 min and then blocked with 1% BSA, glycine in PBS for another 10 min. Primary antibodies (1:1 for anti-UPIII, 1:250 for anti-Rab27b, 1:10 for anti-LAMP-1 and 1:10 for anti-LAMP-2) were incubated with samples at 4°C over night. For Rab27b and CI-MPR staining, after washing with 10 mM glycine in PBS, samples were incubated with 10 nm gold particles conjugated to protein A for 30 min at room temperature and washed again. For UPIII, rabbit anti-mouse IgG was used as second antibody and then incubated with gold-conjugated protein A. For LAMP-1 and LAMP-2 staining, 10 nm gold-conjugated goat anti-rat IgG were used. Sections were fixed in 1% glutaraldehyde in PBS for 5 min to stablize the immunoreaction followed by washing with double-distilled water. After contrasting with neutralized uranyl acetate, 0.4% uranyl acetate/1.8% methylcellulose was used for contrast enhancement and support. The grids were air-dried and analyzed with an electron microscope (JEM 200 CX; JEOL). Bladder tissue was also embedded in Lowacryl K4M (Polysciences, Inc.) (78) and

thin sections were double labeled (see above) using rabbit anti-Rab27b (1:50) and the monoclonal UPIII antibody (undiluted) following essentially published procedures (79).

Western immunoblotting

The urothelial layers were scraped from mouse bladders and homogenized in a buffer containing 50 mM Hepes (pH 7.4), 150 mM NaCl, 1% Triton-X-100 and 5 mM ethylenediaminetetraacetic acid (EDTA) as well as a protease inhibitor cocktail (Roche Applied Science). Fifty micrograms of total proteins was loaded and separated by SDS–PAGE, and then transferred to nitrocellulose membrane (Hybond™-ECL™, Amersham Biosciences). The membranes were incubated with different primary antibodies at 4°C over night. After 3 × washing, secondary antibodies, HRP-conjugated goat anti-mouse IgG, goat anti-rabbit IgG or goat anti-rat IgG were incubated with the membranes. Specific protein bands were visualized by Western Lightning™ chemiluminescence Reagent Plus (PerkinElmer life Sciences, Inc.).

Acknowledgments

We thank Mr Robert Boyd for printing and scanning of EMs and for assembling the low magnification overview EMs and Mr Gerald Jahreis for technical assistance. This work was supported by grants from the National Institute of Health DK-52206 (to G. K.), GM-43583 (to D. D. S.), EY-12104, HL-31698 and HL-51480 (to R. T. S.), and DK-39753 and 52206 (to T.-T. S.). Core facilities were used that were in part supported by the Cancer Center Support Grant CA-16056 to Roswell Park Cancer Institute's National Cancer Institute.

Supporting Information

Additional Supporting Information may be found in the online version of this article:

Figure S1: Low magnification EM of normal mouse bladder urothelium. This overview of the normal urothelium of an 8-week-old mouse was assembled from 12 overlapping low magnification (x5000) pictures using the PHOTOSHOP computer program. The border between the umbrella cells and the underlying intermediate cell layer is indicated by a thin red line. The areas indicated by a box are shown at higher magnification in Figure 3B or S3A.

Figure S2: Low magnification EM of the Buff mouse bladder urothelium. This overview of the urothelium from an 8-week-old Buff mouse was created from 15 overlapping low magnification EMs that were assembled as described in Figure S1. The area indicated in the umbrella cell layer by a box is shown at higher magnification in Figure 2D. The boxed area in the lamina propria part of the section is shown at higher magnification in Figure S3B.

Figure S3: The cytoplasm of Buff mouse bladder fibroblasts is filled with lysosome-like organelles. Higher magnification images of the lamina propria area of the bladder from a normal mouse (A) or from a Buff mouse (B), as indicated by boxes in the low magnification EMs in Figures S1 and S2.

Figure S4: In the Buff mouse, Rab27b and UPIII are associated with immature FVs in the urothelial layer below the umbrella cells. Thin sections of a Buff mouse bladder embedded in Lowacryl K4M were immunogold labeled using an anti-Rab27b antibody (15 nm gold; arrows) and a monoclonal anti-UPIII antibody (5 nm gold; arrow heads). The upper panel shows a low magnification image of the Buff mouse urothelium with the bladder lumen (L) at the upper right side corner and the lamina propria with embedded fibroblasts (F) at the left hand corner. Under the staining conditions used, the umbrella cells filled with MVBs stained consistently much less intensely than the two cell layers below. The high magnification image of the area indicated by a frame in the upper panel shows vesicles containing both Rab27b and uroplakins (UPIII).

References

1. Hicks RM. The fine structure of the transitional epithelium of rat ureter. J Cell Biol 1965;261:25–48.
2. Porter KR, Kenyon K, Badenhausen S. Specializations of the unit membrane. Protoplasma 1967;63:262–274.
3. Liang FX, Bosland MC, Huang H, Romih R, Baptiste S, Deng FM, Wu XR, Shapiro E, Sun TT. Cellular basis of urothelial squamous metaplasia: roles of lineage heterogeneity and cell replacement. J Cell Biol 2005;171:835–844.
4. Staehelin LA, Chlapowski FJ, Bonneville MA. Lumenal plasma membrane of the urinary bladder. I. Three-dimensional reconstruction from freeze-etch images. J Cell Biol 1972;53:73–91.
5. Hicks RM, Ketterer B. Hexagonal lattice of subunits in the thick luminal membrane of the rat urinary bladder. Nature 1969;224:1304–1305.
6. Vergara J, Longley W, Robertson JD. A hexagonal arrangement of subunits in membrane of mouse urinary bladder. J Mol Biol 1969;46:593–596.
7. Walz T, Haner M, Wu XR, Henn C, Engel A, Sun TT, Aebi U. Towards the molecular architecture of the asymmetric unit membrane of the mammalian urinary bladder epithelium: a closed ''twisted ribbon'' structure. J Mol Biol 1995;248:887–900.
8. Kachar B, Liang F, Lins U, Ding M, Wu XR, Stoffler D, Aebi U, Sun TT. Three-dimensional analysis of the 16 nm urothelial plaque particle: luminal surface exposure, preferential head-to-head interaction, and hinge formation. J Mol Biol 1999;285:595–608.
9. Wu XR, Manabe M, Yu J, Sun TT. Large scale purification and immunolocalization of bovine uroplakins I, II, and III. Molecular markers of urothelial differentiation. J Biol Chem 1990;265:19170–19179.
10. Lin JH, Wu XR, Kreibich G, Sun TT. Precursor sequence, processing, and urothelium-specific expression of a major 15-kDa protein subunit of asymmetric unit membrane. J Biol Chem 1994;269:1775–1784.
11. Wu XR, Lin JH, Walz T, Haner M, Yu J, Aebi U, Sun TT. Mammalian uroplakins. A group of highly conserved urothelial differentiation-related membrane proteins. J Biol Chem 1994;269:13716–13724.
12. Wu XR, Medina JJ, Sun TT. Selective interactions of UPIa and UPIb, two members of the transmembrane 4 superfamily, with distinct single transmembrane-domained proteins in differentiated urothelial cells. J Biol Chem 1995;270:29752–29759.
13. Liang FX, Riedel I, Deng FM, Zhou G, Xu C, Wu XR, Kong XP, Moll R, Sun TT. Organization of uroplakin subunits: transmembrane topology, pair formation and plaque composition. Biochem J 2001;355:13–18.
14. Deng FM, Liang FX, Tu L, Resing KA, Hu P, Supino M, Hu CC, Zhou G, Ding M, Kreibich G, Sun TT. Uroplakin IIIb, a urothelial differentiation marker, dimerizes with uroplakin Ib as an early step of urothelial plaque assembly. J Cell Biol 2002;159:685–694.
15. Wu XR, Kong XP, Pellicer A, Kreibich G, Sun TT. Uroplakins in urothelial biology, function, and disease. Kidney Int 2009;75:1153–1165.
16. Tu L, Sun TT, Kreibich G. Specific heterodimer formation is a prerequisite for uroplakins to exit from the endoplasmic reticulum. Mol Biol Cell 2002;13:4221–4230.

17. Hu CC, Liang FX, Zhou G, Tu L, Tang CH, Zhou J, Kreibich G, Sun TT. Assembly of urothelial plaques: tetraspanin function in membrane protein trafficking. Mol Biol Cell 2005;16:3937–3950.
18. Hicks RM. The function of the golgi complex in transitional epithelium. Synthesis of the thick cell membrane. J Cell Biol 1966;30:623–643.
19. Minsky BD, Chlapowski FJ. Morphometric analysis of the translocation of lumenal membrane between cytoplasm and cell surface of transitional epithelial cells during the expansion-contraction cycles of mammalian urinary bladder. J Cell Biol 1978;77:685–697.
20. Lewis SA, de Moura JL. Incorporation of cytoplasmic vesicles into apical membrane of mammalian urinary bladder epithelium. Nature 1982;297:685–688.
21. Truschel ST, Wang E, Ruiz WG, Leung SM, Rojas R, Lavelle J, Zeidel M, Stoffer D, Apodaca G. Stretch-regulated exocytosis/endocytosis in bladder umbrella cells. Mol Biol Cell 2002;13:830–846.
22. Chen Y, Guo X, Deng FM, Liang FX, Sun W, Ren M, Izumi T, Sabatini DD, Sun TT, Kreibich G. Rab27b is associated with fusiform vesicles and may be involved in targeting uroplakins to urothelial apical membranes. Proc Natl Acad Sci U S A 2003;100:14012–14017.
23. Balestreire EM, Apodaca G. Apical epidermal growth factor receptor signaling: regulation of stretch-dependent exocytosis in bladder umbrella cells. Mol Biol Cell 2007;18:1312–1323.
24. Truschel ST, Ruiz WG, Shulman T, Pilewski J, Sun TT, Zeidel ML, Apodaca G. Primary uroepithelial cultures. A model system to analyze umbrella cell barrier function. J Biol Chem 1999;274:15020–15029.
25. Amano O, Kataoka S, Yamamoto TY. Turnover of asymmetric unit membranes in the transitional epithelial superficial cells of the rat urinary bladder. Anat Rec 1991;229:9–15.
26. Zerial M, McBride H. Rab proteins as membrane organizers. Nat Rev Mol Cell Biol 2001;2:107–117.
27. Grosshans BL, Ortiz D, Novick P. Rabs and their effectors: achieving specificity in membrane traffic. Proc Natl Acad Sci U S A 2006;103:11821–11827.
28. Yi Z, Yokota H, Torii S, Aoki T, Hosaka M, Zhao S, Takata K, Takeuchi T, Izumi T. The Rab27a/granuphilin complex regulates the exocytosis of insulin-containing dense-core granules. Mol Cell Biol 2002;22:1858–1867.
29. Gomi H, Mori K, Itohara S, Izumi T. Rab27b is expressed in a wide range of exocytic cells and involved in the delivery of secretory granules near the plasma membrane. Mol Biol Cell 2007;18:4377–4386.
30. Barral DC, Ramalho JS, Anders R, Hume AN, Knapton HJ, Tolmachova T, Collinson LM, Goulding D, Authi KS, Seabra MC. Functional redundancy of Rab27 proteins and the pathogenesis of Griscelli syndrome. J Clin Invest 2002;110:247–257.
31. Starcevic M, Nazarian R, Dell'Angelica EC. The molecular machinery for the biogenesis of lysosome-related organelles: lessons from Hermansky-Pudlak syndrome. Semin Cell Dev Biol 2002;13:271–278.
32. Tolmachova T, Abrink M, Futter CE, Authi KS, Seabra MC. Rab27b regulates number and secretion of platelet dense granules. Proc Natl Acad Sci U S A 2007;104:5872–5877.
33. Marks MS, Seabra MC. The melanosome: membrane dynamics in black and white. Nat Rev Mol Cell Biol 2001;2:738–748.
34. Raposo G, Marks MS. The dark side of lysosome-related organelles: specialization of the endocytic pathway for melanosome biogenesis. Traffic 2002;3:237–248.
35. Bonifacino JS. Insights into the biogenesis of lysosome-related organelles from the study of the Hermansky-Pudlak syndrome. Ann N Y Acad Sci 2004;1038:103–114.
36. Stinchcombe J, Bossi G, Griffiths GM. Linking albinism and immunity: the secrets of secretory lysosomes. Science 2004;305:55–59.
37. Khandelwal P, Ruiz WG, Balestreire-Hawryluk E, Weisz OA, Goldenring JR, Apodaca G. Rab11a-dependent exocytosis of discoidal/fusiform vesicles in bladder umbrella cells. Proc Natl Acad Sci U S A 2008;105:15773–15778.
38. Sato TK, Rehling P, Peterson MR, Emr SD. Class C Vps protein complex regulates vacuolar SNARE pairing and is required for vesicle docking/fusion. Mol Cell 2000;6:661–671.
39. Suzuki T, Oiso N, Gautam R, Novak EK, Panthier JJ, Suprabha PG, Vida T, Swank RT, Spritz RA. The mouse organellar biogenesis mutant buff results from a mutation in Vps33a, a homologue of yeast vps33 and Drosophila carnation. Proc Natl Acad Sci U S A 2003;100:1146–1150.
40. Hermansky F, Pudlak P. Albinism associated with hemorrhagic diathesis and unusual pigmented reticular cells in the bone marrow: report of two cases with histochemical studies. Blood 1959;14:162–169.
41. Di Pietro SM, Dell'Angelica EC. The cell biology of Hermansky-Pudlak syndrome: recent advances. Traffic 2005;6:525–533.
42. Huizing M, Anikster Y, Gahl WA. Hermansky-Pudlak syndrome and related disorders of organelle formation. Traffic 2000;1:823–835.
43. Li W, Rusiniak ME, Chintala S, Gautam R, Novak EK, Swank RT. Murine Hermansky-Pudlak syndrome genes: regulators of lysosome-related organelles. Bioessays 2004;26:616–628.
44. Swank RT, Novak EK, McGarry MP, Rusiniak ME, Feng L. Mouse models of Hermansky Pudlak syndrome: a review. Pigment Cell Res 1998;11:60–80.
45. Piper RC, Katzmann DJ. Biogenesis and function of multivesicular bodies. Annu Rev Cell Dev Biol 2007;23:519–547.
46. Anderson RG, Falck JR, Goldstein JL, Brown MS. Visualization of acidic organelles in intact cells by electron microscopy. Proc Natl Acad Sci U S A 1984;81:4838–4842.
47. Dell'Angelica EC, Mullins C, Caplan S, Bonifacino JS. Lysosome-related organelles. Faseb J 2000;14:1265–1278.
48. Futter CE, Pearse A, Hewlett LJ, Hopkins CR. Multivesicular endosomes containing internalized EGF-EGF receptor complexes mature and then fuse directly with lysosomes. J Cell Biol 1996;132:1011–1023.
49. Vogler C, Rosenberg HS, Williams JC, Butler I. Electron microscopy in the diagnosis of lysosomal storage diseases. Am J Med Genet Suppl 1987;3:243–255.
50. Huizing M, Didier A, Walenta J, Anikster Y, Gahl WA, Kramer H. Molecular cloning and characterization of human VPS18, VPS 11, VPS16, and VPS33. Gene 2001;264:241–247.
51. Gamp AC, Tanaka Y, Lullmann-Rauch R, Wittke D, D'Hooge R, de Deyn PP, Moser T, Maier H, Hartmann D, Reiss K, Illert AL, von Figura K, Saftig P. LIMP-2/LGP85 deficiency causes ureteric pelvic junction obstruction, deafness and peripheral neuropathy in mice. Hum Mol Genet 2003;12:631–646.
52. Eskelinen EL, Tanaka Y, Saftig P. At the acidic edge: emerging functions for lysosomal membrane proteins. Trends Cell Biol 2003;13:137–145.
53. Reczek D, Schwake M, Schroder J, Hughes H, Blanz J, Jin X, Brondyk W, Van Patten S, Edmunds T, Saftig P. LIMP-2 is a receptor for lysosomal mannose-6-phosphate-independent targeting of beta-glucocerebrosidase. Cell 2007;131:770–783.
54. Born M, Pahner I, Ahnert-Hilger G, Jons T. The maintenance of the permeability barrier of bladder facet cells requires a continuous fusion of discoid vesicles with the apical plasma membrane. Eur J Cell Biol 2003;82:343–350.
55. Orci L, Ravazzola M, Amherdt M, Yanaihara C, Yanaihara N, Halban P, Renold AE, Perrelet A. Insulin, not C-peptide (proinsulin), is present in crinophagic bodies of the pancreatic B-cell. J Cell Biol 1984;98:222–228.
56. Marsh BJ, Soden C, Alarcon C, Wicksteed BL, Yaekura K, Costin AJ, Morgan GP, Rhodes CJ. Regulated autophagy controls hormone content in secretory-deficient pancreatic endocrine beta-cells. Mol Endocrinol 2007;21:2255–2269.

57. Tiwari S, Italiano JE Jr, Barral DC, Mules EH, Novak EK, Swank RT, Seabra MC, Shivdasani RA. A role for Rab27b in NF-E2-dependent pathways of platelet formation. Blood 2003;102:3970–3979.
58. Savina A, Vidal M, Colombo MI. The exosome pathway in K562 cells is regulated by Rab11. J Cell Sci 2002;115:2505–2515.
59. Banta LM, Vida TA, Herman PK, Emr SD. Characterization of yeast Vps33p, a protein required for vacuolar protein sorting and vacuole biogenesis. Mol Cell Biol 1990;10:4638–4649.
60. Banta LM, Robinson JS, Klionsky DJ, Emr SD. Organelle assembly in yeast: characterization of yeast mutants defective in vacuolar biogenesis and protein sorting. J Cell Biol 1988;107:1369–1383.
61. Peterson MR, Emr SD. The class C Vps complex functions at multiple stages of the vacuolar transport pathway. Traffic 2001;2:476–486.
62. Poupon V, Stewart A, Gray SR, Piper RC, Luzio JP. The role of mVps18p in clustering, fusion, and intracellular localization of late endocytic organelles. Mol Biol Cell 2003;14:4015–4027.
63. Yu JF, Fukamachi S, Mitani H, Hori H, Kanamori A. Reduced expression of vps11 causes less pigmentation in medaka, Oryzias latipes. Pigment Cell Res 2006;19:628–634.
64. Maldonado E, Hernandez F, Lozano C, Castro ME, Navarro RE. The zebrafish mutant vps18 as a model for vesicle-traffic related hypopigmentation diseases. Pigment Cell Res 2006;19:315–326.
65. Sevrioukov EA, He JP, Moghrabi N, Sunio A, Kramer H. A role for the deep orange and carnation eye color genes in lysosomal delivery in Drosophila. Mol Cell 1999;4:479–486.
66. Pulipparacharuvil S, Akbar MA, Ray S, Sevrioukov EA, Haberman AS, Rohrer J, Kramer H. Drosophila Vps16A is required for trafficking to lysosomes and biogenesis of pigment granules. J Cell Sci 2005;118:3663–3673.
67. Akbar MA, Ray S, Kramer H. The SM protein Car/Vps33A regulates SNARE-mediated trafficking to lysosomes and lysosome-related organelles. Mol Biol Cell 2009;20:1705–1714.
68. Vega MA, Rodriguez F, Segui B, Cales C, Alcalde J, Sandoval IV. Targeting of lysosomal integral membrane protein LIMP II. The tyrosine-lacking carboxyl cytoplasmic tail of LIMP II is sufficient for direct targeting to lysosomes. J Biol Chem 1991;266:16269–16272.
69. Ogata S, Fukuda M. Lysosomal targeting of Limp II membrane glycoprotein requires a novel Leu-Ile motif at a particular position in its cytoplasmic tail. J Biol Chem 1994;269:5210–5217.
70. Sandoval IV, Arredondo JJ, Alcalde J, Gonzalez Noriega A, Vandekerckhove J, Jimenez MA, Rico M. The residues Leu(Ile)475-Ile(Leu, Val, Ala)476, contained in the extended carboxyl cytoplasmic tail, are critical for targeting of the resident lysosomal membrane protein LIMP II to lysosomes. J Biol Chem 1994;269:6622–6631.
71. Wu X, Wang F, Rao K, Sellers JR, Hammer JA III. Rab27a is an essential component of melanosome receptor for myosin Va. Mol Biol Cell 2002;13:1735–1749.
72. Strom M, Hume AN, Tarafder AK, Barkagianni E, Seabra MC. A family of Rab27-binding proteins. Melanophilin links Rab27a and myosin Va function in melanosome transport. J Biol Chem 2002;277:25423–25430.
73. Fukuda M, Kuroda TS, Mikoshiba K. Slac2-a/melanophilin, the missing link between Rab27 and myosin Va: implications of a tripartite protein complex for melanosome transport. J Biol Chem 2002;277:12432–12436.
74. Sarikas SN, Chlapowski FJ. The effect of thioglycolate on intermediate filaments and membrane translocation in rat urothelium during the expansion-contraction cycle. Cell Tissue Res 1989;258:393–401.
75. Riedel I, Czernobilsky B, Lifschitz-Mercer B, Roth LM, Wu XR, Sun TT, Moll R. Brenner tumors but not transitional cell carcinomas of the ovary show urothelial differentiation: immunohistochemical staining of urothelial markers, including cytokeratins and uroplakins. Virchows Arch 2001;438:181–191.
76. Zhao S, Torii S, Yokota-Hashimoto H, Takeuchi T, Izumi T. Involvement of Rab27b in the regulated secretion of pituitary hormones. Endocrinology 2002;143:1817–1824.
77. Marshall J, McEachern KA, Kyros JA, Nietupski JB, Budzinski T, Ziegler RJ, Yew NS, Sullivan J, Scaria A, Van Rooijen N, Barranger JA, Cheng SH. Demonstration of feasibility of in vivo gene therapy for Gaucher disease using a chemically induced mouse model. Mol Ther 2002;6:179–189.
78. Kerr DE, Liang F, Bondioli KR, Zhao H, Kreibich G, Wall RJ, Sun TT. The bladder as a bioreactor: urothelium production and secretion of growth hormone into urine. Nat Biotechnol 1998;16:75–79.
79. Slot JW, Geuze HJ. Cryosectioning and immunolabeling. Nat Protoc 2007;2:2480–2491.